

RESEARCH ARTICLE

WILEY

Extracting angles of attack from blade-resolved rotor CFD simulations

Federico Zilic de Arcos  | Christopher R. Vogel  | Richard H. J. Willden

Department of Engineering Science, University of Oxford, Oxford, UK

Correspondence

Federico Zilic de Arcos, Department of Engineering Science, University of Oxford, Parks Road, Oxford OX1 3PJ, UK.
federico.zilic@eng.ox.ac.uk

Funding information

Engineering and Physical Sciences Research Council, Grant/Award Number: EP/R007322/1; Fondo de Fomento al Desarrollo Científico y Tecnológico, Grant/Award Number: PFCHA/BECAS CHILE DOCTORADO EN EL EXTRANJERO 2016

Abstract

The distribution of the angles of attack over the span of a rotor blade, together with blade element theory, provides a useful framework to understand forces, performance and other fluid dynamic phenomena of axial-flow rotors. However, the angle of attack is not straightforward to define for a three-dimensional rotor, where the flow is perturbed by the blade circulation, shed vorticity and wake development.

This paper evaluates six methods to extract the angles of attack from blade-resolved CFD simulations of axial-flow turbines. Simulations of two different rotors are presented: a low solidity rotor designed for wind and a higher solidity rotor designed for tidal stream energy conversion. Of the analysed methods, five were obtained from the literature and are tested in terms of their internal parameters. The remaining method is named the streamtube analysis method (SAM) and is presented as an improvement on analysis methods that azimuthally average the flow data on the rotor plane, referred to as azimuthal averaging techniques (AATs). The SAM method accounts for the expansion of the streamtubes in flow-field velocity sampling and exhibits improved convergence on the internal parameters compared with AAT.

The six methods are benchmarked in terms of the angles of attack, axial induction factors and the local lift and drag coefficients, identifying that most perform well and converge with each other despite the different underlying assumptions or modelling approaches. However, given the limitations and inherent dependency on internal parameters, the line averaging and SAM are suggested for general flow analysis application.

KEYWORDS

angle of attack, axial flow, flow field analysis, tidal, turbine, wind

1 | INTRODUCTION

The forces on axial-flow turbines are typically characterised through the steady two-dimensional framework described by blade element momentum theory.¹ This model describes the turbine as a disc positioned perpendicular to the flow with no thickness. Its blades are represented as collections of independent aerofoil sections over a finite number of concentric annuli, with the flow through each annulus being homogeneous and the forces on each section considered as functions of the local flow conditions. This two-dimensional framework is a useful model to describe and

This is an open access article under the terms of the Creative Commons Attribution License, which permits use, distribution and reproduction in any medium, provided the original work is properly cited.

© 2020 The Authors. Wind Energy published by John Wiley & Sons Ltd

analyse the performance of axial-flow rotors and has been widely used for turbine design and analysis (see e.g., Burton et al. and ¹ Ning²) despite its limitations in representing three-dimensional flow effects near the tip and the root of the blades (e.g., Glauert³ and Shen et al.⁴) and in misaligned flow conditions. Thus, it is desirable to analyse blade-resolved turbine simulations, experiments and even full-scale rotor flows in similar terms to those described by the blade element momentum theory.

The inverse problem is also relevant. Extracting the spanwise distribution of the lift and drag polars in order to use them with lower order models (see e.g., Wimshurst and Willden⁵) requires resolving the local force vector, extracted by integrating pressure and shear force on the blade surfaces, in terms of a frame of reference defined by the local flow and thus by the local angle of attack.

The problem, however, is non-trivial. The flow around a turbine varies across the azimuthal and axial coordinates, with strong gradients near the blades. Furthermore, the local flow over a specific annular section is the result of the inflow characteristics, the operation of the turbine and the development of the wake, making it difficult to define an undisturbed upstream velocity such as that used for defining lift and drag characteristics in wind tunnel experiments. Finally, the concept of a zero-thickness disc cannot be directly applied to a three-dimensional rotor, so the velocities cannot be extracted at that specific plane.

Given these challenges, several flow analysis methods have been proposed in the literature. One of the first approaches developed is to use an inverse blade element momentum method that entails finding the tangential and axial induction factors to describe the local flow velocity based on the measured thrust and torque distributions and using predetermined two-dimensional lift and drag coefficients along with empirical correction factors (see e.g., Lindenburg⁶).

Hansen et al. proposed the azimuthal averaging technique (AAT), which consists of extracting the azimuthally averaged velocities at different fixed radial coordinates upstream and downstream of the turbine and averaging these to obtain the azimuthally averaged axial and tangential velocities from which the local flow angle can be determined.⁷ This method was tested by Johansen and Sørensen by using the blade-resolved CFD simulations of three different rotors (NREL Phase VI, Tellus 95 kW and LM19.1 500 kW) maintaining a fixed rotational speed and a set of inflow velocities ranging from 7 and 20 m/s. Results of their flow analysis were presented in the form of radially varying lift and drag coefficients⁸ without discussing the flow analysis method details.

Shen et al. introduced an iterative method to analyse the Tellus 95 turbine that considered the flow velocity near the blade to be a combination of the local incident velocity and the perturbations caused by the bound circulation on the blades. The influence from the blades was modelled through lifting-line theory, placing vortices along the blade span with a circulation distribution determined using Kutta–Jowkowski's theorem. The authors compared the method with the AAT and showed good agreement in the midspan in terms of the extracted polar coefficients and also significant sensitivity to the distance between the monitor point and the blade.⁹ This method was then used to evaluate experimental data of the Model Experiments in Controlled Conditions (MEXICO) rotor by Yang et al.¹⁰

Shen et al. proposed another method based on blade surface vortex sheets where a distributed circulation was determined directly from a pressure distribution. This method was also tested using the Tellus 95 kW rotor and proved to be more independent of the position of the monitor points than the lifting-line method through comparison of the results in terms of local lift and drag coefficients.¹¹

Bak et al. proposed fitting two-dimensional pressure distributions extracted from wind tunnel experiments to the pressure distributions extracted at different radial positions along a turbine blade. In their paper, the authors used the pressures extracted at four radial positions from the experiments of a DANAERO NM80 2 MW turbine, fitting the pressure surface data to determine the angle of attack.¹²

The pressure-fitting method was regarded as not being reliable enough by Guntur and Sørensen as it depends on the flow not being separated, in a paper that reviewed four methods using CFD simulations of the MEXICO rotor at three different tip speed ratios (TSRs). Their review also tested the inverse Blade Element Momentum, AAT and a variation of the AAT method that extracts the velocity at the blade rather than the azimuthal average. The paper showed a relatively good agreement between the four described methods in terms of the lift and drag coefficients, but poor agreement when compared with results presented by other authors.¹³

Jost et al. performed a thorough review of four different analysis methods using CFD simulations of the DTU 10 MW and the AVATAR turbines. In their paper, the AAT, the two vortex methods described by Shen et al. and a new method called 'line average' are analysed under steady-state and transient conditions, showing results in the form of lift and drag coefficients, blade span distributions of angles of attack and discussing the differences between the methods under steady- and transient-flow conditions.¹⁴

The line average method takes a closed path around each blade cross section and extracts the velocity around this path, assuming that the influence of the circulation will be negated by averaging the flow velocity components. The method showed a good agreement with AAT on the midspan and a faster response to transient changes.¹⁴

Another method is described by Herraiz et al., where the authors propose that extracting the velocities directly from the bisectrix between two blades will provide an approximation to the undisturbed flow velocity. They demonstrate the validity of the assumption with lifting-line theory, and the method is tested using experiments and simulations of the MEXICO rotor and compared with results published in the literature.¹⁵

Rahimi et al. published another review similar to that published by Jost et al. using the same two rotors but only simulating them under steady-state conditions. As in the other review papers, the authors found a good agreement over the midspan of the blades but discrepancies at the tip and the root. They also identify limitations in the methods associated with wake expansion after the flow passes through the turbine.¹⁶

Even though most methods have a relatively good agreement at high TSRs over the midspan, angle of attack discrepancies of about 1° or 2° can be observed in some papers. Whether this difference is acceptable or not will largely depend on the operational regime of the turbine. Tip and root sections escape also the scope for which the concept of angle of attack can be applied as these regions are significantly influenced by three-dimensional effects. Furthermore, most methods exhibit some kind of convergence limitation. For example, the AAT results are influenced by the distance between the upstream and downstream cuts and the rotor plane. The bound circulation line method described in Shen et al. requires the monitor point to be placed at least two chords from the blade, which can be complicated in high-solidity rotors, and a similar problem is observed with the line average method.

Some methods, such as the inverse Blade Element Momentum and pressure fitting, rely on two-dimensional data, which is not ideal as the lift and drag characteristics can change with radial position.⁵ The circulation-based methods, on the other hand, have inviscid-flow assumptions, and despite demonstrating good performance, a method used to analyse high-quality three-dimensional turbulent CFD simulations should, arguably, be free of lower order model assumptions.

In this paper, a method based on the concept of expanding streamtubes is discussed. This is based on the work from Hunter¹⁷ and is analysed in this paper and proposed as an improvement on the classical AAT. This method works by considering the expansion of the flow while passing through the turbine and interpolating the azimuthally averaged velocities not at a constant radial position as in AAT, but over the corresponding expanding streamtubes. The advantage of this method is an improved convergence, the lack of two-dimensional assumptions and that no smoothing of the data is required after the calculation.

For this benchmark study, two axial-flow turbines were employed: the MEXICO rotor, a widely studied wind turbine, and a higher solidity tidal turbine originally designed for blocked-flow conditions by Schluntz and Willden.¹⁸ Blade-resolved CFD simulation data of these two rotors over a range of TSRs were used to evaluate the different methods in terms of their convergence relative to model parameters, and then, the methods are compared with each other in terms of the angles of attack, the axial induction factors and the inferred lift and drag coefficients.

2 | METHODOLOGY

2.1 | Turbine descriptions

Two axial-flow turbines were employed in this work to test the different methods of determining radially varying angles of attack: a tidal rotor optimised for a blocked-flow condition with high solidity and high thrust^{18,19} designated as Sch15B and the test rotor used during MEXICO, a wind turbine for which considerable experimental and numerical data have been published.^{20,21}

The tidal rotor is a three-bladed turbine designed by Schluntz and Willden¹⁸ and further modified by Wimshurst and Willden¹⁹ and Zilic de Arcos et al.²² This rotor has a diameter of 20 m and was optimised to operate under a blocked-flow condition with a blockage, defined as the ratio of turbine swept area to channel cross-sectional area, of $B = 19.6\%$. This rotor uses the RISØ A1-24 aerofoil aligned along the blade's quarter chord.

The MEXICO turbine is a three-bladed wind rotor with a diameter of 4.5 m designed for an FP5 project partly funded by the European Commission. Its blades were comprised of three different aerofoils (DU-91-W2-250, RISØ A1-21 and NACA64-418) with transition regions between them. The simulations used in this work consider a fixed pitch angle of -2.3° .¹⁹

The two turbines were analysed at three TSRs, λ , covering a wide range of cases, 4.0, 5.5 and 7.0 with a variable rotational speed and a fixed inflow of 4.5 m/s for the Sch15B turbine and 4.17, 6.67 and 10.00 with a fixed rotational speed of 424.5 rpm and variable inflow speed for the MEXICO rotor.

Details of the rotors are summarised in Table 1, and the chord and twist characteristics are plotted in Figure 1. The reader should note how the tidal turbine features a larger chord over the blade span as a consequence of its blockage-oriented design. A render comparison of the two rotors is also provided in Figure 2.

TABLE 1 Main design and operational parameters of the Sch15B and MEXICO rotors, displaying type of turbine, number of blades Z , diameters \varnothing , rotational speed ω , original design tip speed ratio λ_D and velocity V_D , simulated tip speed ratios λ , flow velocities V_∞ and chord-based Reynolds number $Rn_{0.75}$ evaluated at $r/R=0.75$

Turbine	Type	Z	Rotor \varnothing (m)	Hub \varnothing (m)	ω (rpm)	λ_D	V_D (m/s)	λ	V_∞ (m/s)	$Rn_{0.75}$
Sch15B	Tidal	3	20.00	3.00	Variable	5.5 ^a	2.0	4.0, 5.5 & 7.0	4.5	$\sim 16 - 31 \times 10^6$
MEXICO	Wind	3	4.50	0.54	424.50	6.7	15.0	10.00, 6.67 & 4.17	10, 15 & 24	$\sim 0.5 \times 10^6$

Abbreviation: MEXICO, Model Experiments in Controlled Conditions.

^aDesign tip speed ratio with a blockage of $B = 0.196$.

FIGURE 1 Approximate chord and twist distributions presented as functions of the non-dimensional radial position, r/R , for the Sch15B and MEXICO rotors. MEXICO, Model Experiments in Controlled Conditions [Colour figure can be viewed at wileyonlinelibrary.com]

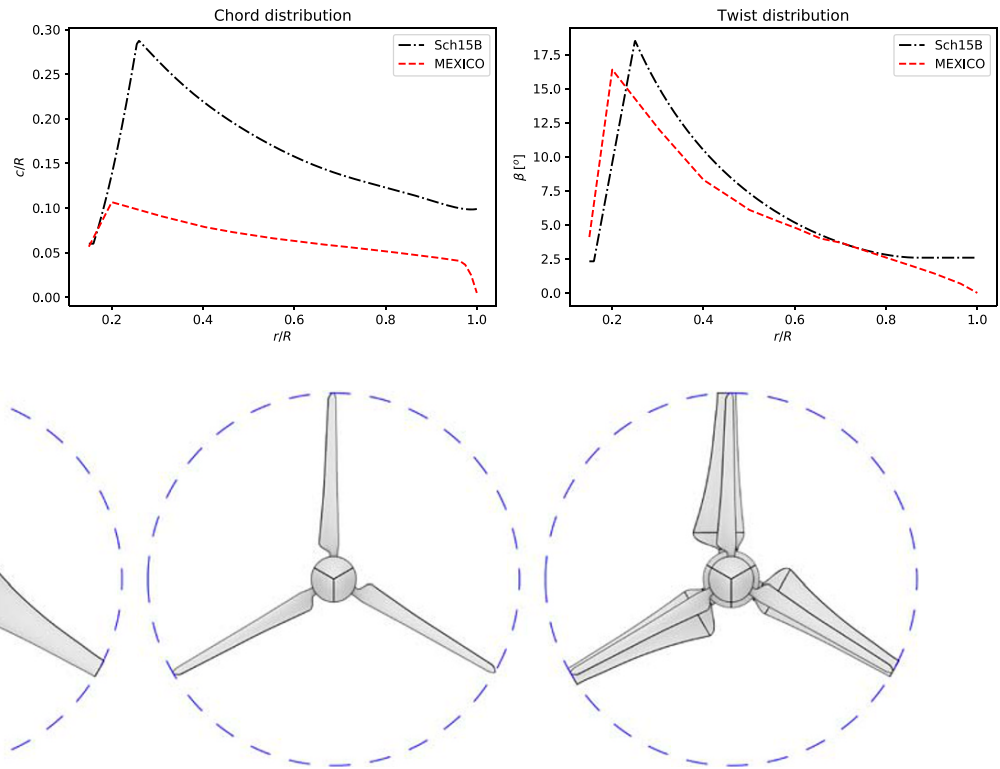


FIGURE 2 Comparison of the Sch15B (left), MEXICO rotor (middle) and an overlay of both rotors (right). Geometries are non-dimensionalised by the corresponding rotor radius. MEXICO, Model Experiments in Controlled Conditions [Colour figure can be viewed at wileyonlinelibrary.com]

2.2 | Numerical models

The data sets employed for this study come from steady-state Reynolds-averaged Navier–Stokes (RANS) CFD simulations. The blade rotation was modelled in both cases using the multiple reference frame approach (MRF),²³ and the $k - \omega$ SST turbulence model²⁴ with updated constants²⁵ was used to close the RANS equations.

The data sets were generated for different research projects, and hence, there are differences in the CFD strategies employed. The Sch15B rotor was simulated with the commercial code Fluent 19.0 with second-order upwind discretisation scheme and a coupled-pressure algorithm, whereas the MEXICO rotor was simulated with OpenFOAM 2.3.1 and the SIMPLE algorithm for pressure–velocity coupling. In both cases, the residuals were reduced by at least five orders for the velocity components and typically five orders for the turbulence scalars.

Structured meshes were employed in both cases. Non-dimensional wall distances of $30 < y^+ < 300$ for the Sch15B and $y^+ < 5$ for the MEXICO rotors were defined, employing an enhanced wall modelling approach for the first case²⁶ and a wall resolved boundary layer on the second. More details of the simulations can be found in Zilic de Arcos et al.²⁷ and Wimshurst and Willden⁵ for the Sch15B and MEXICO rotors, respectively.

2.3 | Flow field analysis methods

2.3.1 | Azimuthal averaging technique

This method operates by obtaining the azimuthally averaged flow speeds at different radial coordinates and axial distances from the rotor plane. Differences in the implementations stem from where the analysis sections are drawn and interpolated between to obtain the velocity at the turbine plane while avoiding the steep velocity gradients that arise on the rotor plane.

The interpolation can be done in different ways. The most straightforward way is to define an arbitrary fixed distance upstream and downstream and average the velocities. Another approach is to describe the velocities as functions of the axial coordinate and to use data at multiple points to perform a higher order interpolation.

Once the axial and tangential velocity components have been extracted, the inflow angle ϕ can be calculated as

$$\phi = \tan^{-1}(V_X/V_T) \quad (1)$$

$$W = \sqrt{V_X^2 + V_T^2}, \quad (2)$$

with V_X and V_T the axial and tangential velocity components, respectively, as obtained from the analysis method utilised.

Despite some authors assigning V_T to be equal to ωr ,^{13,28} with ω the rotational speed and r the local radius, the present work considers the tangential induction factor a' such that

$$V_T = \omega r(1 + a'). \quad (3)$$

The influence of the tangential induction factor, a' , is not significant in the midboard and outboard regions of the blades. However, near the root and where the rotational speed is lower, a' can generate some non-negligible variations in the angle of attack.

Once the inflow angle, ϕ , has been determined, the angle of attack is calculated by subtracting the twist angle β :

$$\alpha = \phi - \beta. \quad (4)$$

In this work, the velocities were extracted by calculating the mean of the azimuthally averaged velocities at planes located upstream and downstream of the turbine plane, at distances x/c expressed as functions of the local chord c and the axial coordinate x .

Applying the AAT analysis process to the CFD simulations, a sensitivity analysis was performed with the results plotted in Figure 3 in terms of the angle of attack for the Sch15B and MEXICO rotors at the analysed operational cases. The MEXICO turbine was analysed with monitor distances from $x/c = 0.25$ to $x/c = 4.0$, whereas the tidal turbine was limited to a maximum $x/c = 2.0$ as, due to its large chord at the root sections, using any value larger than this meant extracting data at a distance that was regarded as being too far from the turbine plane.

From the convergence plots, a spread of about 0.5° is observed, but no convergence with x/c is observed. It is noteworthy that, for the high-TSR cases where the angles of attack are small, the relative error of this spread is in the order of 25%–30%.

2.3.2 | Vortex sheet method

This method is part of a family of techniques that assume the flow velocity to be the sum of the undisturbed velocity and a velocity induced by the turbine's circulation. Hence, if the turbine circulation-induced velocity U_I can be estimated, the undisturbed velocity can be calculated by subtracting the induced component from the velocity at a measuring point located on the turbine's plane.

Shen et al. introduced a method to calculate the induced velocity U_I by modelling the turbine using lifting-line theory.⁹ This method requires the force distribution over the blade span, the lift component that provides a circulation distribution and the velocity at different measuring points. The induced velocity is calculated from the Biot–Savart law and is then subtracted from the measured velocity to calculate the inflow angle ϕ , iterating until convergence is achieved. The method, despite showing promising results, exhibits a dependency on the chordwise location of the measuring points. Shen et al. recommended placing the measuring points at a distance of at least two chords, which might not be practical in some cases.

Shen et al. presented another method based on potential flow theory, introduced as an improvement to the lifting-line method. This method, instead of modelling each blade as a vortex line, employs vortex sheets to model the blade surfaces, thus considering the chordwise distribution of the circulation and reducing solution dependency on the chordwise distance.¹¹ This method is of an increased complexity in comparison with the one presented by Shen et al. as it requires the pressure distribution over the blade sections and, according to the authors, identification of the stagnation and separation points. However, as they describe it to have a better performance, this method will be analysed in this study as the most complete potential flow analysis method.

Method description

The method requires the velocities at different measuring points located on the turbine plane, as well as the pressure distribution over the corresponding sections. Assuming the pressure to be constant through the boundary layer, the velocity at its edge U_t is calculated using Bernoulli's equation:

$$p + \frac{1}{2}\rho|U_t|^2 = p_\infty + \frac{1}{2}\rho U_\infty^2, \quad (5)$$

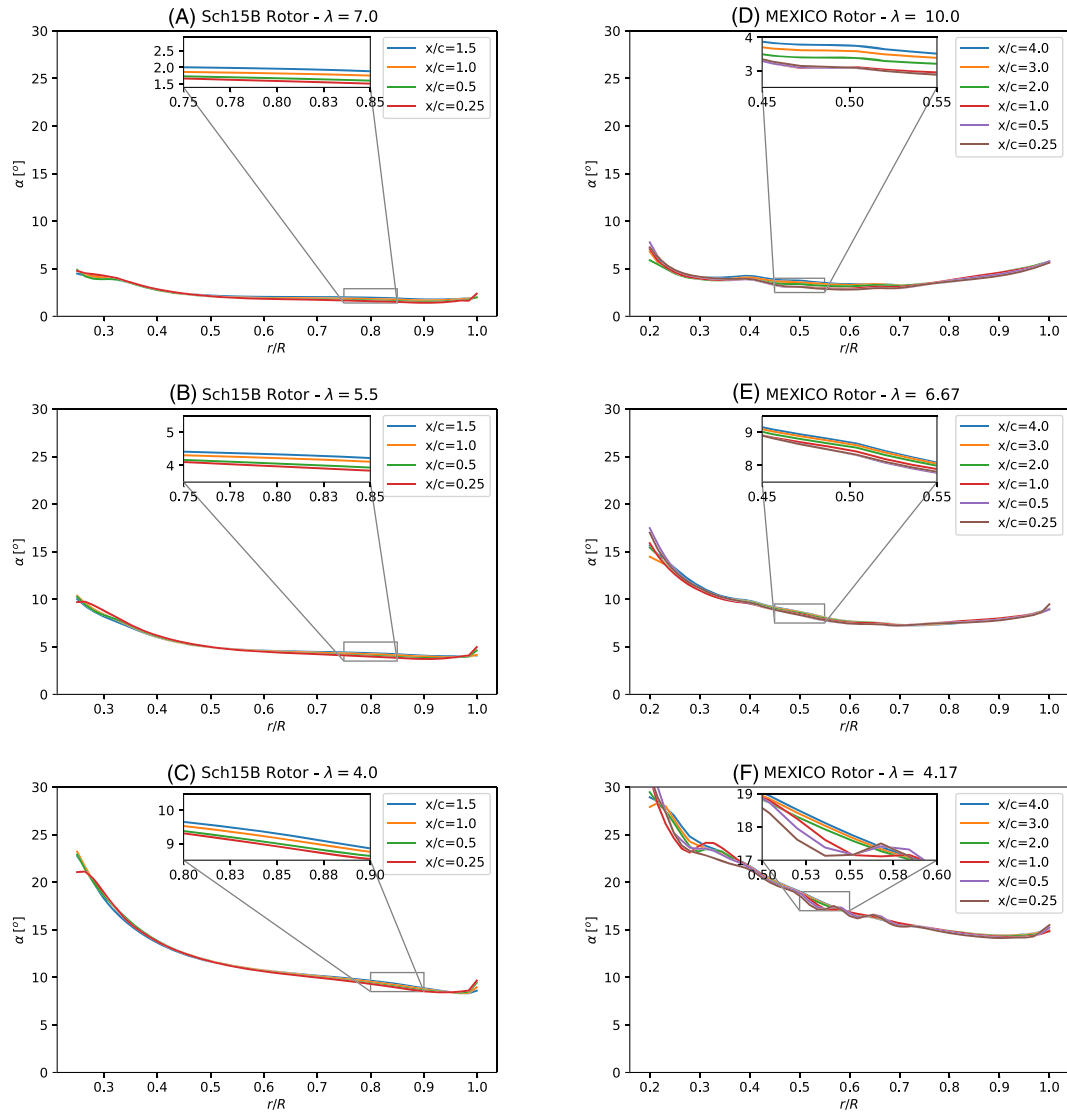


FIGURE 3 Angles of attack obtained with the azimuthal averaging technique method with different monitor positions, x/c , for three different tip speed ratios: (A) $\lambda=7.0$, (B) $\lambda=5.5$ and (C) $\lambda=4.0$, for Sch15B, and (D) $\lambda=10.0$, (E) $\lambda=6.67$, (F) $\lambda=4.17$ for MEXICO. MEXICO, Model Experiments in Controlled Conditions [Colour figure can be viewed at wileyonlinelibrary.com]

with $p-p_\infty$ the pressure at a point on the blade surface and $U_\infty = (V_\infty^2 + \omega^2 r^2)^{1/2}$ the relative flow speed at a certain radial position r and V_∞ the undisturbed flow velocity. Then, the edge velocity is calculated as

$$U_r = U_\infty \sqrt{1 - \frac{2(p-p_\infty)}{\rho U_\infty^2}}, \quad (6)$$

which is used to calculate the local bound circulation density at different points around the cross section as a velocity jump over the boundary layer:

$$\vec{\gamma}(\vec{y}) = \delta U|_{wall} \vec{e}_r = \pm (U_r - 0) \vec{e}_r, \quad (7)$$

where $\delta U|_{wall}$ is the velocity change through the boundary layer and \vec{e}_r is a unitary radial vector aligned with the blade spanwise axis.

Shen et al. indicate that the sign of the bound circulation density should be defined according to the location of the stagnation and separation points: positive between the stagnation and the separation points, negative between the stagnation point and the trailing edge along the pressure surface and, finally, negative between the separation point and the trailing edge. Nonetheless, we consider that this suction surface post-separation sign change is inconsistent with the development of this model, which will be discussed below.

With the circulation defined, the induced velocity is computed using the Biot–Savart law, integrating numerically in both the chordwise and spanwise directions for each blade:

$$\vec{U}_\Gamma(\vec{x}) = \frac{1}{4\pi} \sum_{i=1}^Z \iint_S \frac{\vec{\gamma}(\vec{y}) \times (\vec{x} - \vec{y})}{|\vec{x} - \vec{y}|^3} d\tau dr, \quad (8)$$

with Z the number of blades, S the blade surface, \vec{y} the coordinates of a point on the blade section, \vec{x} the coordinates of the flow analysis point where the velocity is measured, $d\tau$ the chordwise and dr the radial directions.

Then, the undisturbed velocity used to calculate the angle of attack is obtained by subtracting the induced velocity from the velocity at the measuring point $\vec{U}_{MP}(\vec{x})$:

$$\vec{U}(\vec{x}) = \vec{U}_{MP}(\vec{x}) - \vec{U}_\Gamma(\vec{x}). \quad (9)$$

Finally, the inflow angle and the angle of attack can be calculated according to Equations (1) and (4), respectively.

Shen et al. state that the separation point should be identified and, from that point to the trailing edge, the local bound circulation density should become negative.¹¹ Most turbines are not designed to operate with a detached flow because of the transient phenomena associated with this regime and the reduced predictive capacity of CFD, potential flow and Blade Element Momentum techniques. If separation occurs on a turbine under normal operation, it would typically occur over a very limited portion of the blade. Nonetheless, for the MEXICO turbine operating at $\lambda=4.17$, the separated region occupies most of the suction surface, as can be seen in Figure 4.

The assumption of the circulation changing sign after separation occurs results from the observation that the surface flow direction reverses after the separation point and beneath the separated shear layer. However, as the edge velocity, defined previously, only applies outside the shear layer, which is above the separation bubble, we consider that this assumption is not valid. Considering the change in tangential velocity from the wall to above the separated shear layer, the net circulation should still remain positive despite the circulation being negative immediately adjacent to the wall. Hence, there should be no change in the sign of the circulation density.

Furthermore, it is worth noting that the sign change makes no significant difference in the results for other cases except for the MEXICO rotor at the lower TSR analysed and, to a lesser extent, to the $\lambda=6.67$ case. Figure 5 shows a comparison of the angle of attack without correction and the two approaches with regards to the circulation. Additionally, the results obtained with the streamtube analysis method (SAM), presented in Section 2.4, are provided for comparison. From the figure, it can be seen how correcting for the post-separation circulation improves the agreement with the alternative method, which samples directly from the flow field and makes no assumption about separation.

As previously stated, the circulation method requires the velocity at a monitoring point. Shen et al.¹¹ suggest that the Vortex Sheet method should not be sensitive to the location of this point, whereas the bound circulation line method presented in Shen et al. requires at least two chords of separation to the sampling point.⁹

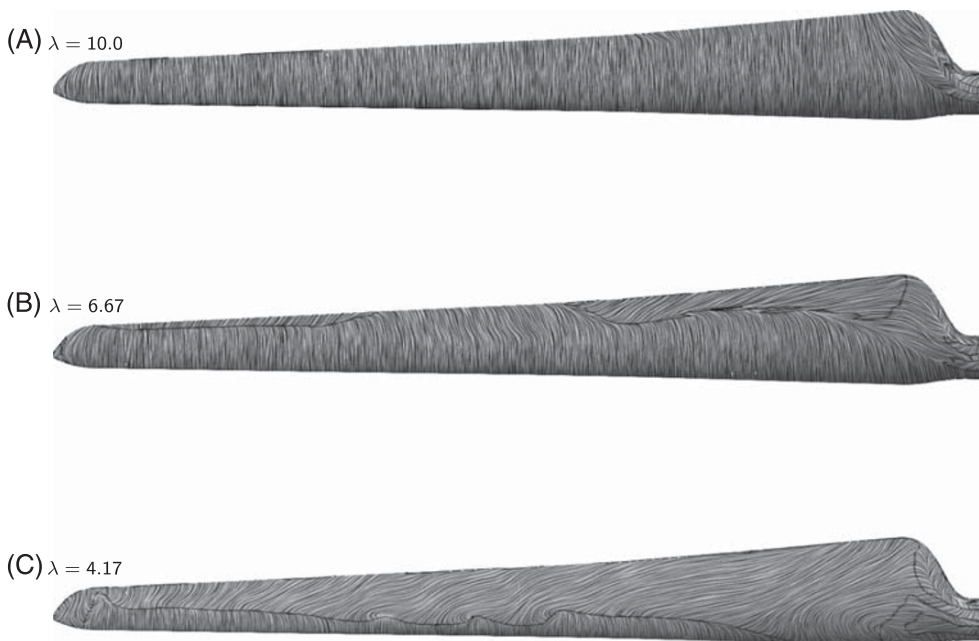


FIGURE 4 Streamlines over the suction surface of the Model Experiments in Controlled Condition rotor plotted using the line integral convolution technique, with the black line highlighting the approximate location where separation occurs. The three analysed tip speed ratios are displayed

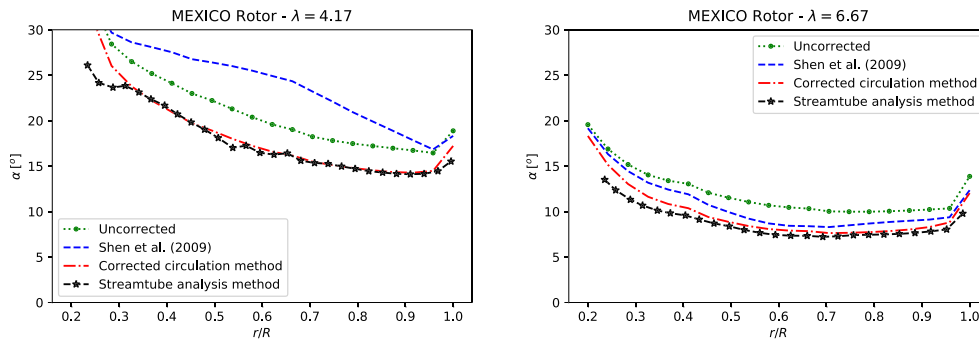
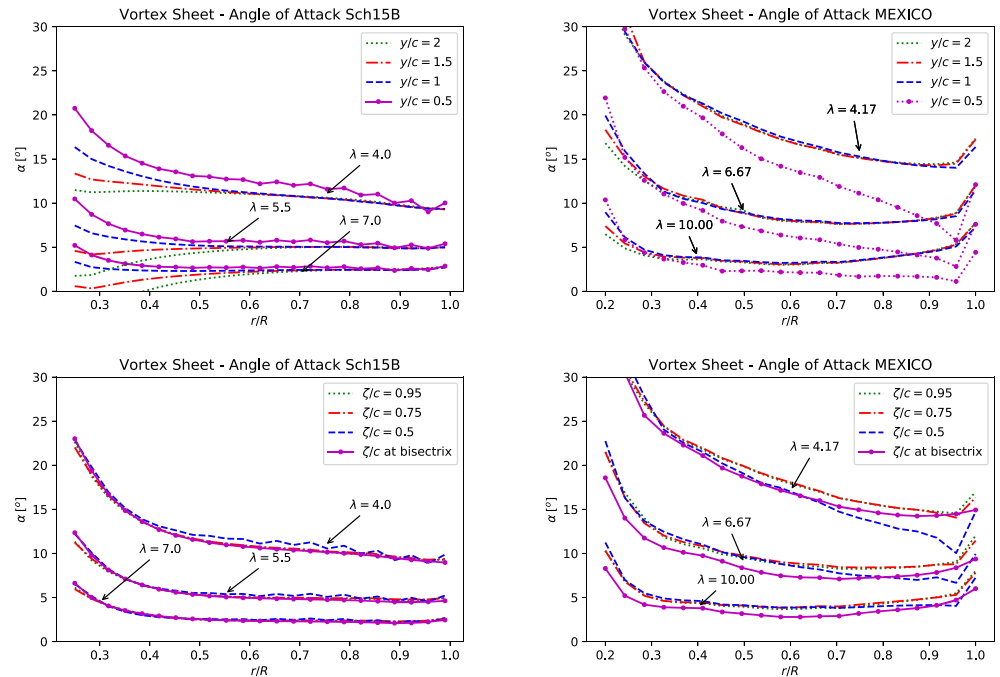


FIGURE 5 Computed angle of attack for the MEXICO turbine at tip speed ratios of 4.17 and 6.67. Lines shown are for angles of attack derived from the flow field without considering velocity induction (uncorrected), with velocity induction correction derived from Shen et al.'s model, with the post-separation correction to the circulation method, and using an alternative streamtube analysis method (see Section 2.4). MEXICO, Model Experiments in Controlled Conditions [Colour figure can be viewed at wileyonlinelibrary.com]

FIGURE 6 Convergence study of the vortex sheet method. Results are presented for the linear, y/c , and the arc segment, ζ/c , distances to the monitor point. MEXICO, Model Experiments in Controlled Conditions [Colour figure can be viewed at wileyonlinelibrary.com]



In the present work, we tested the sensitivity of the vortex sheet method to the location of the monitor points by placing them immediately in front of the analysed section and over the rotor plane to upstream chordwise distances y/c of 0.5, 1.0, 1.5 and 2.0, as shown in Figure 6. Although good convergence between the different cases is seen for the case of the MEXICO rotor for $y/c \geq 1.0$, errors occur when $y/c = 0.5$ due to the local distortion of the flow field and associated large velocity gradients close to the blade. The inclusion of a core radius model may further improve this singularity-based method.²⁹ A significant divergence in the root section is also observed for the Sch15B rotor when distances are presented in terms of y/c . This divergence is a consequence of the high solidity of the rotor, where at an upstream distance of two chords (measured aligned with the local chord), the radial coordinate of the measuring point has substantially changed.

As an improvement, the monitor points can be placed at a constant radius and the chordwise distance projected over the constant-radius arc ζ . This limits the distance at which the monitor points can be placed near the root for a high-solidity turbine, as the points quickly fall into the next blade. Hence, the analysis was performed placing the monitoring points at ζ/c values of 0.5, 0.75, 0.95 and, as a special case, over the bisectrix between two consecutive blades (thus, at varying ζ/c with r/R). The results in Figure 6 show good agreement at the root section for the Sch15B turbine, eliminating the problem seen using a linear chordwise extrapolation to the monitoring points, with some spread in results for $\zeta/c = 0.5$ associated with the local flow perturbation caused by the blade, which is particularly apparent for the low λ case. For the MEXICO rotor, similar divergence of results are seen for low sampling distances and also for analysis using the bisectrix as this is now a large number of chords from the blade for this lower solidity rotor.

2.3.3 | Pressure fitting

This method was originally described by Bak et al. and entails fitting two-dimensional pressure coefficient distributions to the surface pressure fields extracted from three-dimensional simulations. The method was developed as an approach to process experimental data but can also be used to analyse blade-resolved CFD simulation data. Despite being disregarded by Guntur and Sørensen,¹³ this method is included in the analysis.

The original authors state that, to implement the method, the pressure should be fitted only to the pressure side of the blades, where separation is unlikely to occur. Then, the least squares method can be applied to minimise the value of a residual S by varying the angle of attack α and the inflow velocity W :

$$S = \sum_{i=1}^n \left(P_i - \frac{1}{2} \rho W^2 C_{pres}(\chi_i/c, \alpha) \right)^2, \quad (10)$$

with χ/c the non-dimensional chordwise coordinate, n the number of points along the chord where pressure data are available at a given radius r , P_i the pressure as measured at the i th point, ρ the flow density, W the inflow velocity and C_{pres} the pressure coefficient as a function of the position of the point χ_i/c and the angle of attack α .

In this analysis, it is worth noting that the Sch15B turbine consists of a single RISØ A1-24 aerofoil, whereas the MEXICO rotor comprises three different aerofoils with corresponding transition regions. The analysis presented herein covers the entire Sch15B turbine, but was limited to the NACA 64-418 aerofoil, which is used from 74.4% of the span up to the tip on the MEXICO rotor.

The two-dimensional pressure coefficient distributions C_{pres} were extracted from two-dimensional simulations following the CFD configuration described in Section 2.2, using high-quality structured meshes made with ICEM 19.0. Three different meshes were tested for each aerofoil, showing negligible variations and leading to a final cell count of about 3.9×10^5 for the NACA and 2.0×10^5 for the RISØ aerofoils. The simulations were conducted for angles of attack from -20° up to 60° in steps of 1° , and intermediate pressure distributions were obtained by linear interpolation.

The results of the pressure fitting process can be seen, for two typical blade sections, in Figure 7. Good agreement is observed between the two-dimensional CFD data and the pressure field extracted from the blade-resolved rotor CFD. This method, despite showing promise across the blade midspan where the flow is well attached and largely two-dimensional, has significant problems where the flow separates and due to the assumption that the flow is two-dimensional, where three-dimensional effects distort the blade pressure fields from those of two-dimensional aerofoil sections (Wimshurst and Willden⁵).

2.3.4 | Bisectrix

This method, introduced by Herraes et al., works on the assumption that a location on the turbine plane exists where the effects caused by the blades circulation are balanced resulting in net zero velocity induction, allowing the flow velocities to be directly extracted from the flow field.¹⁵

For a uniform axial-flow condition, Herraes et al. prove using the Biot-Savart theorem and a description of the blades based on lifting-line theory, that the velocities sampled at the bisectrix between two consecutive blades are free from any blade induction effects (see Figure 8 for bisectrix location definition).

The main virtue of this approach is its inherent simplicity: it just requires sampling the axial and tangential velocities from the flow (V_x and V_T) and employing these to directly calculate the angles of attack (Equations 1 and 4) without any further manipulation. However, a limitation is that any non-homogeneity in the flow, such as environmental turbulence or boundary-layer shear effects, is neglected, which would negatively impact the extracted results.

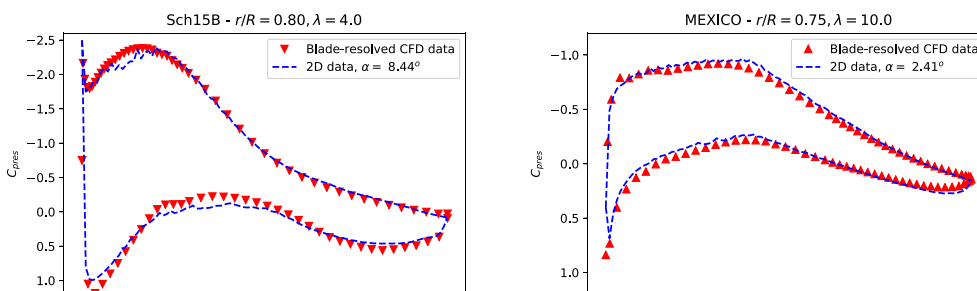


FIGURE 7 Examples of the pressure-fitting technique applied to two arbitrary cases for the Sch15B (left) and MEXICO (right) rotors. MEXICO, Model Experiments in Controlled Conditions [Colour figure can be viewed at wileyonlinelibrary.com]

FIGURE 8 Schematics of the velocity extraction regions in the bisectrix (left) and line average methods (right) [Colour figure can be viewed at wileyonlinelibrary.com]

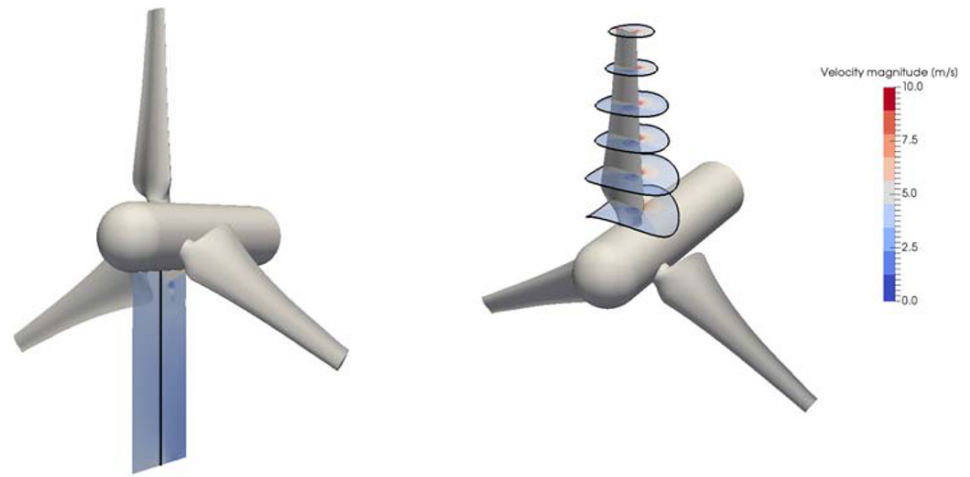
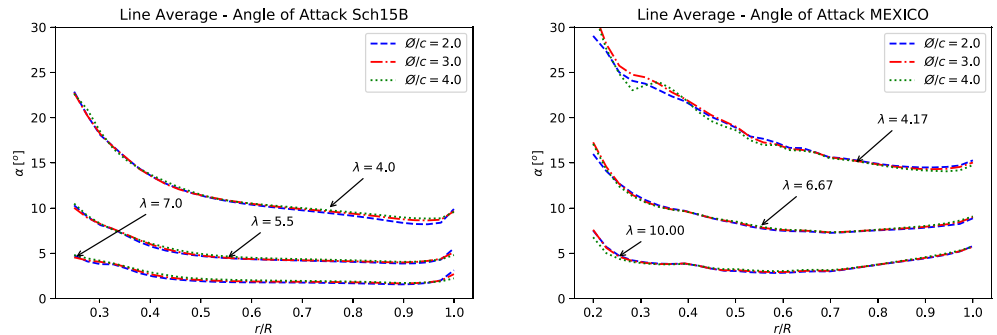


FIGURE 9 Angles of attack obtained from the velocities averaged around closed circular pathlines enclosing the local blade as a function of pathline diameter, \varnothing/c , for the Sch15B and MEXICO rotors at the three tip speed ratios. MEXICO, Model Experiments in Controlled Conditions [Colour figure can be viewed at wileyonlinelibrary.com]



2.3.5 | Line average

Jost et al. introduced this method, which works with a similar circulation-based framework as others previously discussed. It assumes that each blade section produces a circulation effect that can be removed from the flow field to obtain the inflow angles.¹⁴ Despite using a similar underlying assumption to other methods discussed, this method does not directly model the blade as a set of bound vortices to obtain the induced velocity, but averages the velocity components V_x and V_T over a symmetric closed pathline centred on the blade quarter chord for different radial positions, as shown schematically in Figure 8. As the average is taken around the blade, not only does the circulation influence vanish, but the method should also be capable of capturing local and even transient effects.

The major drawback of the method is associated with trailing vorticity, which, if captured around the pathline averages, can negatively influence the accuracy of the results. For this reason, the method was tested with circular pathlines projected over constant radii, and a convergence study was performed extracting the angles of attack for the two rotors under different conditions, using different radii pathlines expressed as a function of the local chord c . The results can be seen in Figure 9, showing that the method is almost invariant to variations in the pathline radius used to enclose the blade sections in the midspan sections, with some small divergence of the results observed at the tip and root of the blades.

2.4 | Streamtube analysis method

The concept of using the SAM to extract the angles of attack and the flow velocity components at the turbine plane was originally developed by Hunter¹⁷ in an attempt to improve the convergence of the traditional AATs by additionally considering the expansion of the streamtube in the velocity extraction process. In common with the line average and bisectrix methods, this approach has the advantage of taking the data directly from the flow and not requiring any form of post-processing or smoothing. However, the definition of a streamtube in a viscous flow is not as straightforward as in momentum theory. When a viscous flow passes through a turbine, it develops fast local gradients, vortices of different scales and a wake that will experience mixing and exchange energy with the surrounding fluid.

In the viscous-flow scenario, the behaviour of the flow past a turbine can be analysed using sets of independent streamlines seeded over the azimuth at a constant radius. In Appendix B1, we provide more details on the streamlines behaviour, tracking their radial position and showing a low spread from the average radial position. The streamlines analysis, expensive in computational terms, shows that the streamtubes can be approximated to have a circular cross section of radius $R_S(x)$ tangent to the azimuthally averaged flow speed. This approach is introduced in the

next section as a simplified and more practical method, as well as less expensive in computational resources, to build the tube surface using the azimuthal averages of the axial and radial flow speeds, in a similar way to the AAT but integrating these velocities in the axial direction to obtain the expanding streamtube surface. A comparison of both the streamlines and streamtubes approach is also provided in Appendix B1, showing an excellent agreement except near the tip where strong gradients and three-dimensional flow effects dominate.

2.4.1 | Azimuthally averaged streamtubes

Assuming the streamtubes to maintain a circular cross section, as detailed in Appendix B1, we can numerically integrate the azimuthally averaged radial and axial velocities to construct a set of streamtube surfaces. For the case of steady-state simulations, we can define the streamlines as a function of the axial coordinate x . Defining V_X and V_R to be the azimuthally averaged axial and radial velocity components, respectively, and as introduced in Section 2.3.1, and noting the streamtube of radius R_S will be tangent to the local flow, we may write

$$\frac{dR_S}{dx} = \frac{V_R(x, r)}{V_X(x, r)} \quad (11)$$

$$\Rightarrow R_S(x) = \int \frac{V_R}{V_X} dx, \quad (12)$$

which can be solved numerically as a function of x for any given value of r , as shown schematically in Figure 10 for a first-order numerical integration method.

Once the streamtubes have been reconstructed, the averaged velocity components over the streamtube $R_S(x)$ (i.e., at varying radial positions) can be used to calculate the angle of attack as described in Section 2.3.1. This requires interpolating upstream and downstream along the identified streamtube to extract the velocities either side of the turbine plane. The same first-order interpolation scheme as used in Section 2.3.1 is employed to interpolate along the streamtube. The full approach is summarised in Algorithm 1.

Algorithm 1 Reconstruction of the azimuthally averaged streamtubes

```

Define x values // Set of axial coordinates
Define  $r_0$  values // Initial radii at  $x_0$ 
 $i = 0$ 
 $j = 1$ 
for  $i$  do // Loop across radii
   $r = r_{i,0}$ 
  for  $j$  do // Loop across axial positions
    Extract  $V_X(r_{ij}, x_i)$ 
    Extract  $V_R(r_{ij}, x_i)$ 
    Calculate  $r_{i,j+1} = f(V_X, V_R)$  // (See e.g., Figure 10)
     $j = j + 1$ 
  end for
  Define the streamtube  $R_S(x)$  as the collection of  $r_i$  points
  Extract velocities to calculate  $\alpha$ 
   $i = i + 1$ 
end for

```

The streamtubes reconstruction approach is tested by integrating the velocities using first- and fourth-order Runge–Kutta methods, each with axial steps of $\Delta x/R = 1/30$ and $\Delta x/R = 1/60$, for $x/R \in [-0.5, +0.5]$. The results from this analysis are shown in Figure 11 in the form of a set of streamtubes for the Sch15B rotor at two operational conditions, showing little variation between the four different cases except in zones near the tip, where the strong gradients are better captured by the higher order integration scheme. In Figure 12, the results for the different integration schemes and $\Delta x/R$ values are presented for the MEXICO and Sch15B rotors in terms of the angle of attack distribution α , also showing a good agreement between the cases except near the tip.

Finally, the streamtube method sensitivity to x/c is analysed on the same basis as the AAT method in Section 2.3.1, that is, at the same values that were used, and the results are plotted in Figure 13. From these plots, it can be observed that the spread of α is reduced in the inboard

FIGURE 10 First order numerical integration scheme to obtain the azimuthal-averaged streamtubes [Colour figure can be viewed at wileyonlinelibrary.com]

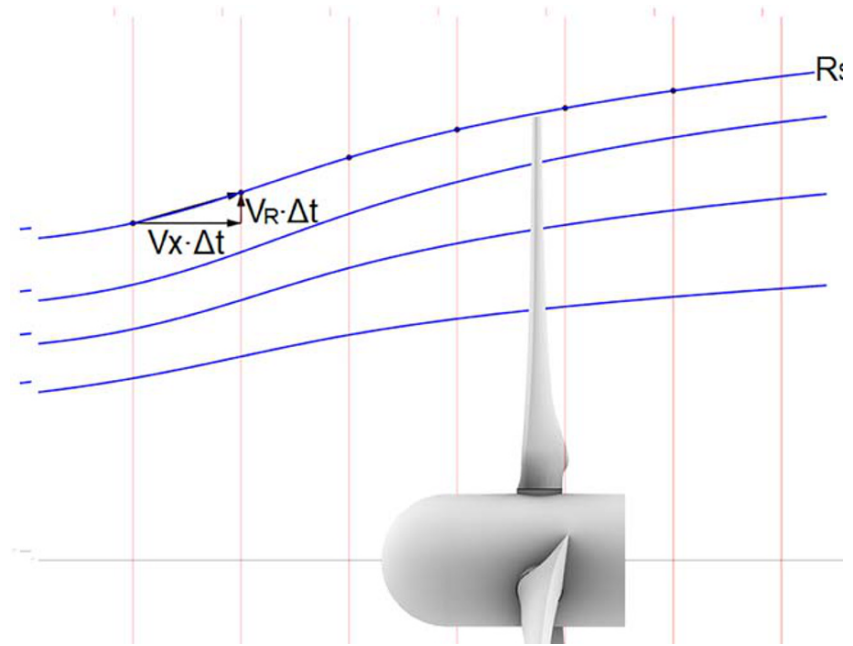


FIGURE 11 Streamtube reconstruction for the Sch15B rotor using first- and fourth-order Runge–Kutta methods (labelled as RK1 and RK4, respectively) and axial resolutions $\Delta x/R$ for tip speed ratios of 4.0 and 7.0 [Colour figure can be viewed at wileyonlinelibrary.com]

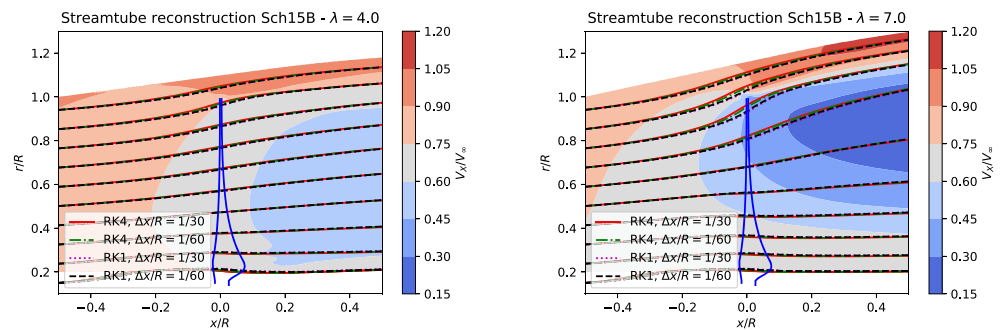
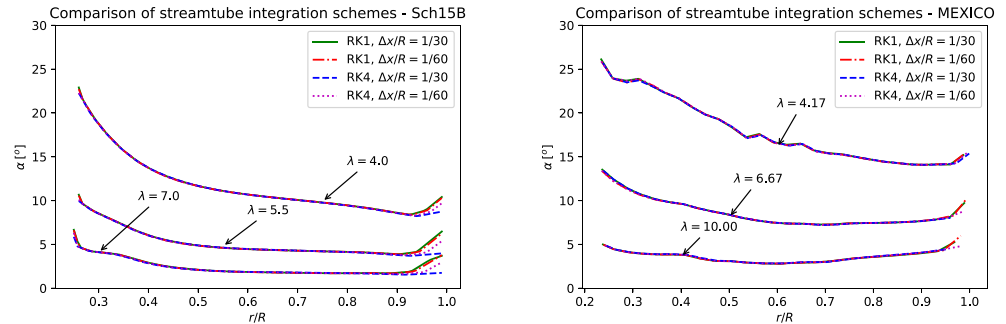


FIGURE 12 Comparison of the angles of attack calculated with the streamtube analysis method using first- and fourth-order Runge–Kutta integration schemes and different step sizes $\Delta x/R$. MEXICO, Model Experiments in Controlled Conditions [Colour figure can be viewed at wileyonlinelibrary.com]



sections and root proximities when compared with the AAT, whereas some variations with x/c can still be observed towards the tip. The reduction in spread of α , and therefore insensitivity to x/c , is particularly apparent for the lower solidity MEXICO rotor for higher TSRs where the flow remains attached.

3 | BENCHMARK AND DISCUSSION

The concept of α is non-trivial to define for a rotating blade in three dimensions, and hence, it is not possible to conclusively validate the methods with reference to any metric. Instead, this analysis evaluates how the different methods converge with each other in terms of three different variables: the spanwise distribution of the angle of attack α , the spanwise distribution of the axial induction factor a and the local lift and drag coefficients at two radial positions (from the computed relationship between angle of attack and normal and tangential force coefficients), one in the

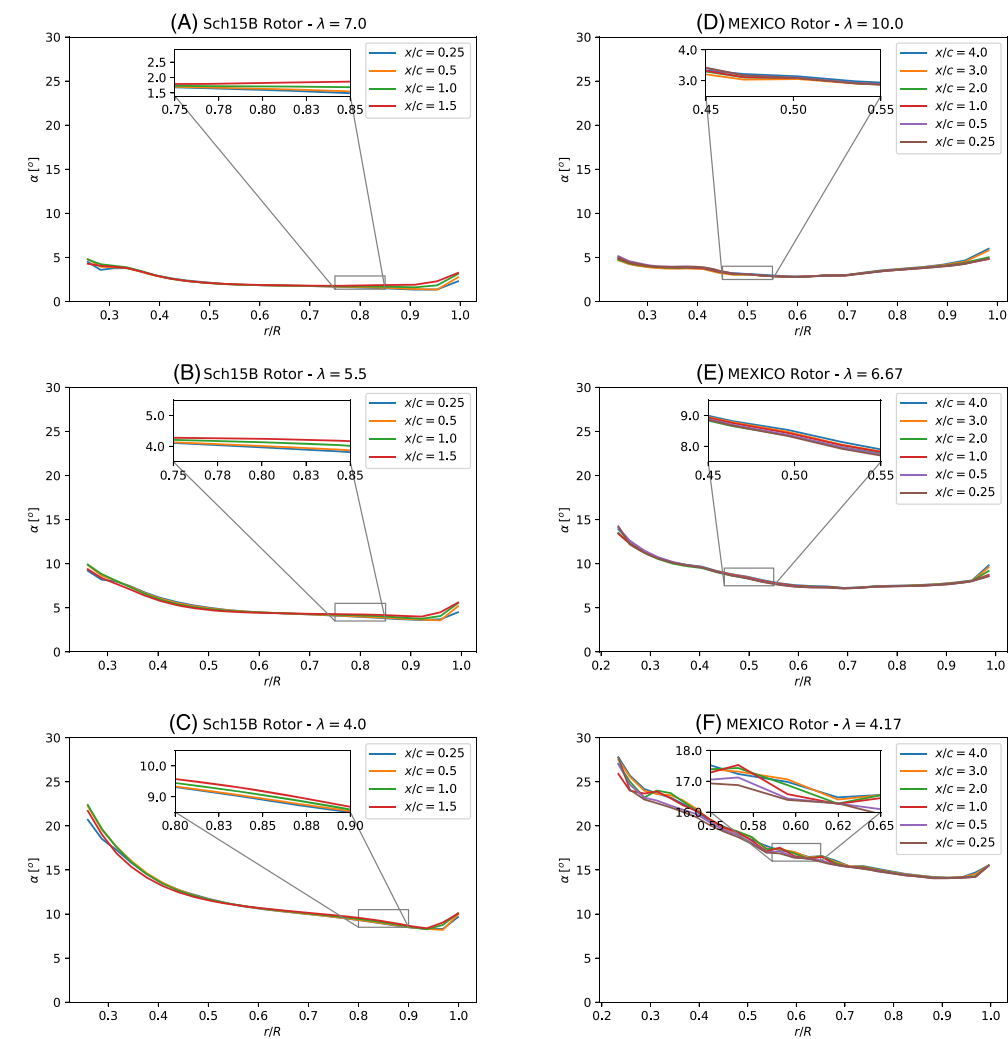


FIGURE 13 Angles of attack obtained with the streamtube analysis method with different data probing values, x/c , for three different tip speed ratios: (A) $\lambda = 7.0$, (B) $\lambda = 5.5$ and (C) $\lambda = 4.0$, for Sch15B, and (D) $\lambda = 10.0$, (E) $\lambda = 6.67$, (F) $\lambda = 4.17$ for MEXICO. MEXICO, Model Experiments in Controlled Conditions [Colour figure can be viewed at wileyonlinelibrary.com]

TABLE 2 Parameters used by different methods for the benchmarking exercise

		AAT	SAM	Vortex sheet	Line average	Pressure	Bisectrix
Sch15B	Parameter	x/c	x/c	ζ/c	\emptyset/c	Side	-
	value	1.00	1.00	0.95	2.00	Pressure side	-
MEXICO	Parameter	x/c	x/c	y/c	\emptyset/c	Side	-
	value	1.00	1.00	1.5	2.00	Pressure side	-

^aAbbreviations: AAT, azimuthal averaging technique; MEXICO, Model Experiments in Controlled Conditions; SAM, streamtube analysis method.

midspan region and one close to the tip, providing different levels of detail and error masking. Each method is presented for a representative case of internal model variables. Typically, the presented case should be for a converged value (where convergence can be achieved), and the details are presented in Table 2.

Notice in Table 2 that two different variables for the MEXICO and Sch15B rotors were used to assess the vortex sheet method. This is because we considered the selected variables and their respective values that achieve the best performance of the method for each rotor, as presented in Section 2.3.2.

3.1 | Angles of attack

The angles of attack are the first set of results to be analysed as they are the key focus of the current work. In Figure 14, the reader will note that most methods converge with each other quite well even though they are based on very different assumptions and theories, with the pressure method being the outlier.

FIGURE 14 Angles of attack computed using various analysis methods for two rotors, Sch15B and MEXICO, at various tip speed ratios. AAT, azimuthal averaging technique; MEXICO, Model Experiments in Controlled Conditions; SAM, streamtube analysis method [Colour figure can be viewed at wileyonlinelibrary.com]

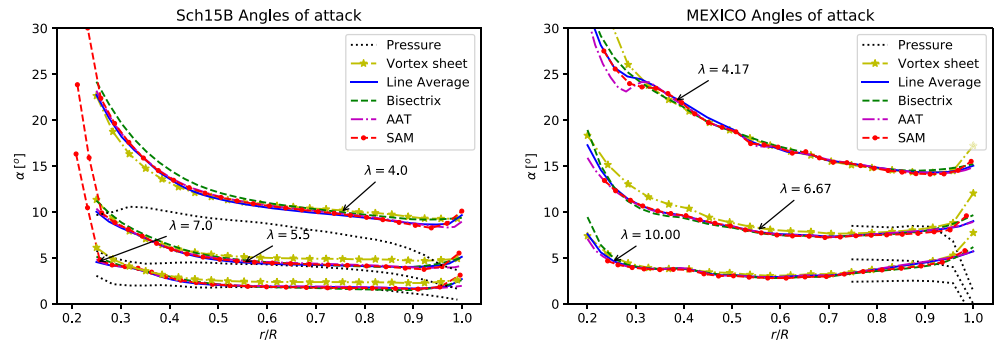
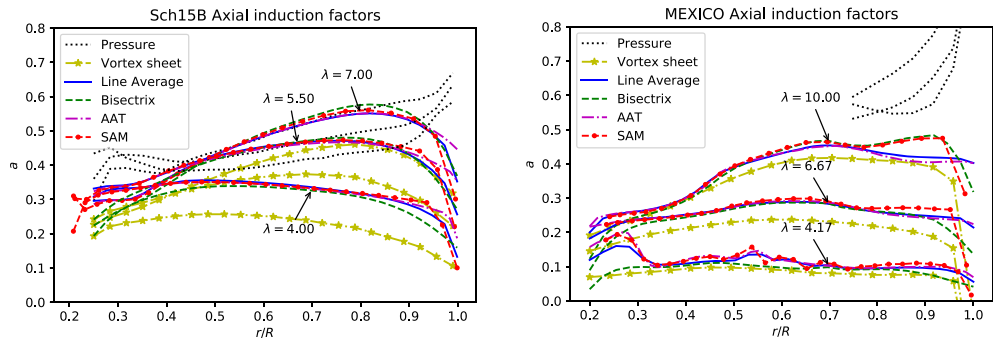


FIGURE 15 Axial induction factors computed using various analysis methods for two rotors, Sch15B and MEXICO, at various tip speed ratios. AAT, azimuthal averaging technique; MEXICO, Model Experiments in Controlled Conditions; SAM, streamtube analysis method [Colour figure can be viewed at wileyonlinelibrary.com]



The pressure method had already been reported by Guntur and Sørensen¹³ as not being reliable, and the present analysis agrees with their conclusion. The pressure method displays good agreement in the midspan region for the TSRs of 7.0 and 5.5 for the Sch15B rotor, where the flow behaves mostly as two-dimensional, with no separation and at relatively low angles of attack. However, outside of this well behaved region, the results diverge from other methods considerably. A similar trend is observed for the MEXICO rotor, even though the data are more limited; recall that only the NACA profile occupying the outer region of the blade is analysed here.

The vortex sheet method diverges slightly from the rest of the methods in some of the cases, without observing a specific pattern, but even when running on a completely different theoretical basis, it still displays a good agreement with the rest of the analysed methods. The bisectrix method also shows some minor differences, especially for the Sch15B case at higher angles of attack and between the midspan and blade root. This is due to the higher local blade solidity of the inboard region, which is more pronounced for this turbine. This high local solidity is sufficient to perturb the flow as far as the local bisectrix, rendering the assumption of undisturbed flow, once lifting line effects mutually cancel along the bisectrix, invalid.

3.2 | Axial induction factors

Blade angles of attack are generally small and subject to small angle differences between analysis methods, partially due to the dominance of the rotational velocity component in determining the inflow angle. It is therefore instructive to examine the different analysis method calculations of the axial induction factor, defined according to Equation (13) and plotted in Figure 15.

$$a = 1 - V_x/V_\infty \quad (13)$$

The induction factors uncover more significant differences in the calculations. They show a significant divergence of the vortex sheet method from the other methods, which was masked in the angle of attack analysis. This is likely due to the inviscid nature of the vortex sheet method considering the circulation around the blades and does not fully capture viscous drag effects. The drag contributes significantly to overall thrust and thus flow deceleration. The lack of drag considerations in the vortex sheet model leads to an overestimation of through rotor flow speed and thus an underestimation of the induction factor. The error is higher for the Sch15B rotor than the MEXICO rotor, due to the higher thrust loading of the former.

The figure also shows how the bisectrix method diverges near the root, departing from the other solutions as the bisectrix gets closer to the blades and their influence becomes stronger, as discussed previously. Note also how the AAT, SAM and line average methods maintain relatively

good agreement with each other, with the exception of the tip regions, where three-dimensional flow effects dominate, and at higher TSRs where thrust tends to be higher, increasing the wake expansion and the three-dimensional effects at the outboard blade sections. Those three methods also appear to capture some of the separation-induced effects on the MEXICO rotor at $\lambda = 4.17$ around the midspan, which manifest as wiggles or rapid spanwise changes in induction factor.

3.3 | Force coefficients

The lift and drag coefficients at different radii can be used as a metric to evaluate different methods (see e.g., Johansen and Sørensen,²⁸ Shen⁹ and Guntur and Sørensen¹³). First, the distributions of thrust and tangential force per unit length, F_X and F_T , respectively, are extracted from the CFD simulations by integrating the pressure and shear forces over a finite number of blade slices normal to the blade axis.^{5,27} These forces are then resolved into components parallel and normal to the local flow to yield blade sectional lift and drag coefficients:

$$C_L = \frac{L'}{1/2\rho W^2 c}, \quad (14)$$

$$C_D = \frac{D'}{1/2\rho W^2 c}, \quad (15)$$

where L' and D' are the sectional lift and drag forces, respectively.

In this analysis, we consider two radial positions; one at the midspan region ($r/R = 0.65$), where a small spread is seen between the angles of attack provided by the analysed methods, and one at the near tip region ($r/R = 0.97$) where the spread is larger. Each simulation is analysed to yield single lift and drag coefficients at the corresponding radial position using the local angle of attack. Simulations at multiple TSRs are used to generate dependency with angle of attack. The results of this analysis can be seen in Figures 16 and 17 for the Sch15B and MEXICO rotors, respectively.

Disregarding the pressure-fitting method for the moment, we note that the spread between the computed coefficients is low even for the $r/R = 0.97$ cases on the two rotors. As with the previous analysis, it can be seen that some divergence is present for the vortex sheet method but still exhibits the same general trend as the other methods.

From this analysis technique, it is difficult to draw further conclusions, as force coefficient analysis masks the error sources. Recalling Equations (14) and (15), it is noted that the flow analysis methods differ in the calculation of W , which is dominated by the $V_T \approx \omega r$ component, and by the trigonometric relationship between the rotor-based frame of reference (thrust and torque) and the flow-based frame of reference (lift and drag).

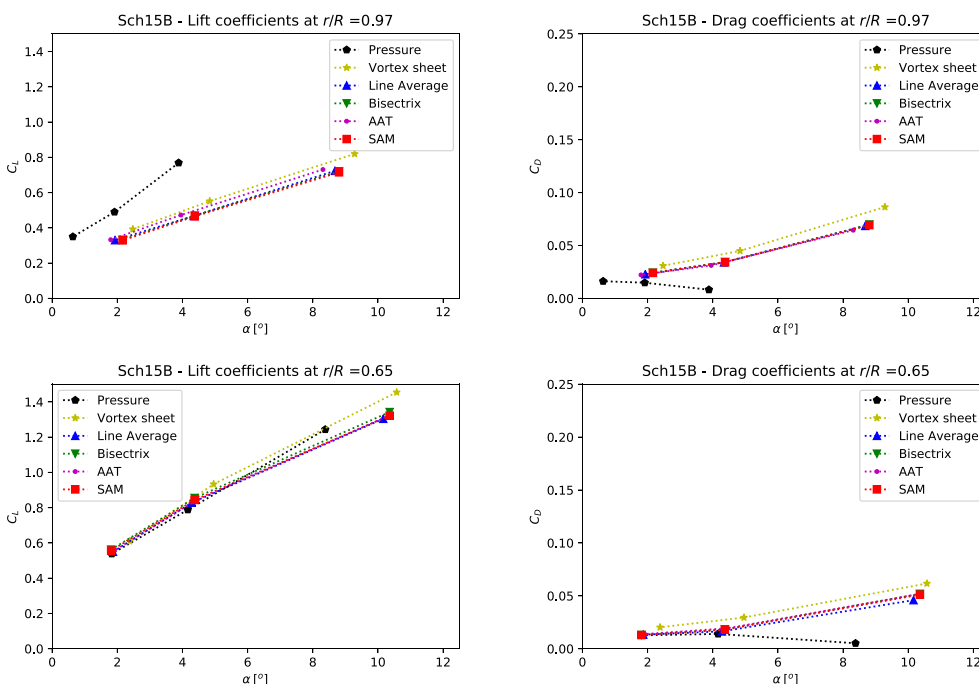
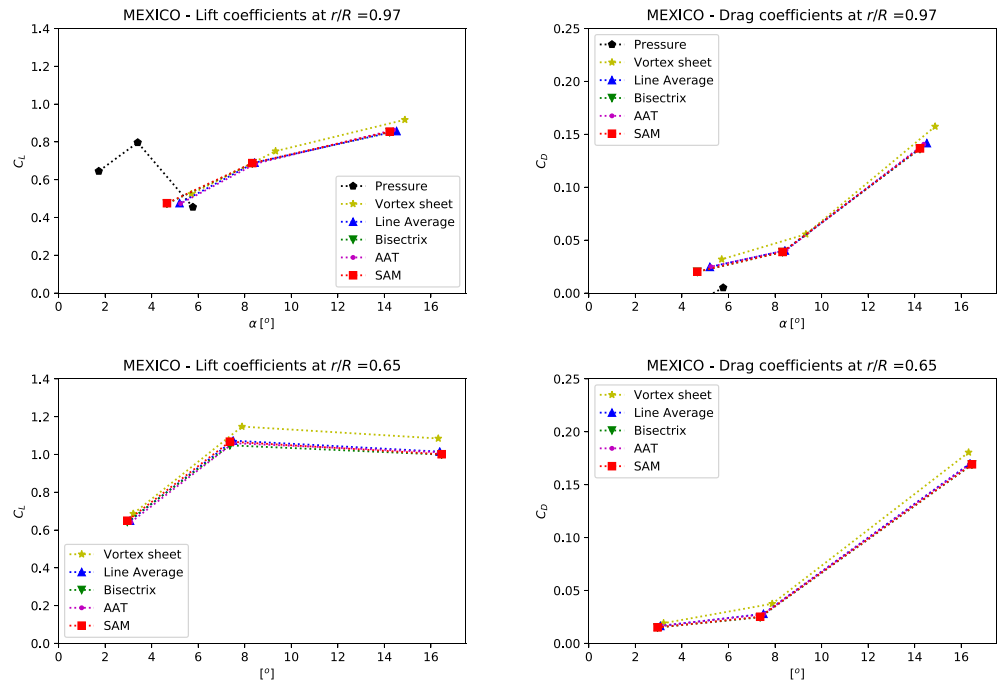


FIGURE 16 Sectional lift and drag coefficients for the Sch15B rotor. AAT, azimuthal averaging technique; MEXICO, Model Experiments in Controlled Conditions; SAM, streamtube analysis method [Colour figure can be viewed at wileyonlinelibrary.com]

FIGURE 17 Sectional lift and drag coefficients for the MEXICO rotor. AAT, azimuthal averaging technique; MEXICO, Model Experiments in Controlled Conditions; SAM, streamtube analysis method [Colour figure can be viewed at wileyonlinelibrary.com]



The trigonometric relationship between the two different frames of reference depends on the inflow angle ϕ and not directly on α . Despite the absolute error for α and ϕ are the same (the difference between α and ϕ being the local blade twist angle β), ϕ is generally larger than α especially at high twist (inboard) regions of the blade, and thus, the relative error passed to the force calculations will be lower.

Comparison of the local lift and drag coefficients inferred from each model demonstrates that in certain applications, the variations in coefficients determined by the different flow analysis methods may be negligible.

4 | CONCLUSIONS

This work has analysed six different methods based on different underlying assumptions to extract the angle of attack from three-dimensional blade-resolved CFD simulations. These methods are based variously on circulation theory, streamtube interpolation and least squares fitting of two-dimensional surface pressures. Five of the six methods analysed showed good agreement with each other in calculating the spanwise distribution of angle of attack, particularly over the midspan of the two rotors analysed in this work. The pressure method was the only exception, which has also been reported to provide inaccurate results in other studies.¹³

Although the remaining methods generally performed well, a number of limitations arising from their underlying assumptions and the physics of rotor blades were identified. The strong radial-flow velocity components and trailing vortices, which arise near blade tips, render two-dimensional concepts such as angle of attack less appropriate, and hence, these regions should not be treated in the same way as the rest of the blade. However, as the angle of attack calculation is dominated by the tangential speed, the spread between different models in the tip region tends to be small. The differences between methods were highlighted by comparing the axial induction factor.

The vortex sheet method is developed from potential flow hypotheses and thus models the turbine under inviscid assumptions. It was found that, after correcting the post-separation assumption in the original method,¹¹ better alignment of the predicted axial induction factor was achieved between this and the other flow analysis methods for the MEXICO rotor than it was achieved for the Sch15B rotor. The lower solidity and thrust characteristics of the former rotor result in a smaller flow perturbation that in turn requires smaller flow correction.

The line average and bisectrix methods showed good agreement in all of the analysed flow metrics. Of the two methods, we consider that the first is preferable as the latter could be significantly affected by ambient flow conditions such as environmental turbulence and shear. Both methods are influenced by the shed vortices and other blade-generated flow phenomena, especially near the root. This can be especially significant for high solidity rotors.

The SAM provided improved performance over the AAT in terms of the internal parameter x/c , reducing uncertainty in the computed flow field values. Furthermore, the analysis of the streamtubes can also provide a valuable tool in exploring the flow phenomena around a rotor more generally, such as understanding near-rotor wake development.

Although it is not possible to conclusively validate the accuracy of the methods with respect to an independent model of angle of attack variation, we consider that the SAM and the line average methods are the most appropriate for general applications. They both have low sensitivity

to their internal parameters (x/c and \varnothing/c respectively), demonstrate good agreement with the other methods evaluated, work by directly sampling the flow field and are relatively straightforward to implement.

ACKNOWLEDGEMENTS

This work was supported in part by CONICYT PFCHA/BECAS CHILE DOCTORADO EN EL EXTRANJERO 2016 /72170292. RHJW would like to acknowledge EPSRC who support his fellowship through grant EP/R007322/1. The authors would also like to acknowledge the use of the University of Oxford Advanced Research Computing (ARC) facility in carrying out this work. <https://doi.org/10.5281/zenodo.22558>.

ORCID

Federico Zilic de Arcos  <https://orcid.org/0000-0002-4236-9039>

Christopher R. Vogel  <https://orcid.org/0000-0003-2232-9811>

REFERENCES

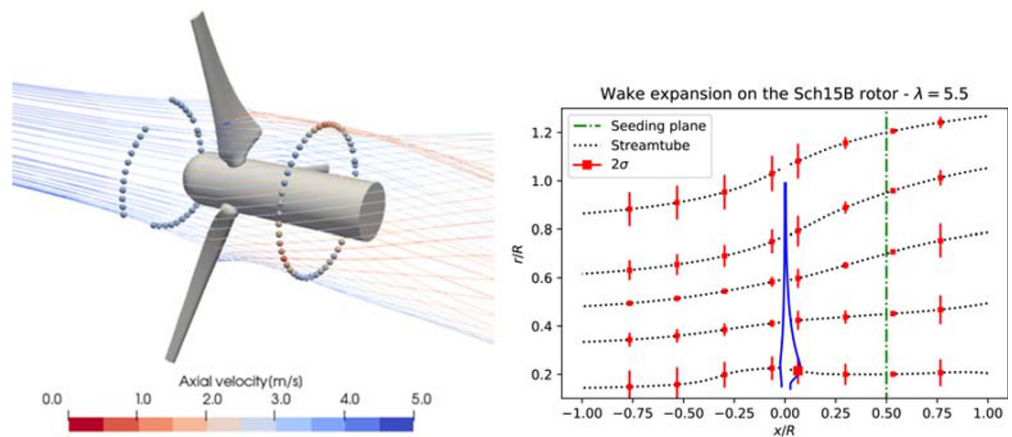
- Burton T, Jenkins N, Sharpe D, Bossanyi E. *Wind Energy Handbook*: Chichester, United Kingdom: Wiley; 2011.
- Ning SA. A simple solution method for the blade element momentum equations with guaranteed convergence. *Wind Energy*. 2014;17(9):1327-1345.
- Glauert H. *Airplane Propellers*: Berlin, Germany: Springer; 1935.
- Shen WZ, Mikkelsen R, Sørensen JN, Bak C. Tip loss corrections for wind turbine computations. *Wind Energy: An Int J Prog Appl Wind Power Conv Technol*. 2005;8(4):457-475.
- Wimshurst A, Willden RHJ. Extracting lift and drag polars from blade-resolved computational fluid dynamics for use in actuator line modelling of horizontal axis turbines. *Wind Energy*. 2017;20(5):815-833. <http://doi.wiley.com/10.1002/we.2065>
- Lindenbarg C. Investigation into rotor blade aerodynamics. Energy research Centre of the Netherlands (ECN) Wind Energy publication, ECN-C-03-025; 2003.
- Hansen MOL, Sørensen NN, Michelsen JA. Extraction of lift, drag and angle of attack from computed 3-d viscous flow around a rotating blade. In: European Wind Energy Conference; 1997.
- Hansen MOL, Johansen J. Tip studies using CFD and comparison with tip loss models. *Wind Energy*. 2004;7(4):343-356.
- Shen WZ, Hansen MOL, Sørensen JN. *Determination of Angle of Attack (AOA) for Rotating Blades*, *Wind Energy: Proceedings of the Euromech Colloquium*. Berlin Heidelberg; 2006.
- Yang H, Shen WZ, Sørensen JN, Zhu WJ. Extraction of airfoil data using PIV and pressure measurements. *Wind Energy*. 2011;14:539-556.
- Shen WZ, Hansen MOL, Sørensen JN. Determination of the angle of attack on rotor blades. *Wind Energy*. 2009;12(1):91-98.
- Bak C, Troldborg N, Madsen H. DAN-AERO MW : Measured airfoil characteristics for a MW rotor in atmospheric conditions. In: Scientific Proceedings: European Wind Energy Association; 2011:171-175.
- Guntur S, Sørensen NN. An evaluation of several methods of determining the local angle of attack on wind turbine blades. *J Phys Conf Ser*. 2014;555(1):012045.
- Jost E, Klein L, Leipprand H, Lutz T, Krämer E. Extracting the angle of attack on rotor blades from CFD simulations. *Wind Energy*. 2018;21(10):807-822.
- Herráez I, Daniele E, Schepers JG. Extraction of the wake induction and angle of attack on rotating wind turbine blades from PIV and CFD results. *Wind Energy Sci*. 2018;3(1):1-9.
- Rahimi H, Schepers J, Shen WZ, et al. Evaluation of different methods for determining the angle of attack on wind turbine blades with CFD results under axial inflow conditions. *Renew Energy*. 2018;125:866-876. 1709.04298.
- Hunter W. Actuator disk methods for tidal turbine arrays. *Ph.D. Thesis*; 2015.
- Schluntz J, Willden R. The effect of blockage on tidal turbine rotor design and performance. *Renew Energy*. 2015;81:432-441.
- Wimshurst A, Willden RHJ. Computational analysis of blockage designed tidal turbine rotors. In: Progress in Renewable Energies Offshore - Proceedings of 2nd International Conference on Renewable Energies Offshore, RENEW 2016; 2016:587-597.
- Snel H, Schepers J, Montgomerie B. The MEXICO project (model experiments in controlled conditions): the database and first results of data processing and interpretation. *J Phys Conf Ser*. 2007;75(1):012014.
- Bechmann A, Sørensen NN, Zahle F. CFD simulations of the Mexico rotor. *Wind Energy*. 2011;14(5):677-689.
- Zilic de Arcos F, Vogel C, Willden RHJ. Hydroelastic modelling of composite tidal turbine blades. In: Advances in Renewable Energies Offshore: Proceedings of the 3rd International Conference on Renewable Energies Offshore (RENEW 2018); Lisbon, Portugal:877.
- Luo J, Gosman A. Prediction of impeller-induced flow in mixing vessels using multiple frames of reference. INSTITUTE OF CHEMICAL ENGINEERS SYMPOSIUM SERIES; 1994.
- Menter FR. Two-equation eddy-viscosity turbulence models for engineering applications. *AIAA J*. 1994;32(8):1598-1605.
- Menter FR, Kuntz M, Langtry R. Ten years of industrial experience with the SST turbulence model. *Turbul Heat Mass Trans* 4. 2003;4:625-632.
- Fluent A. *Ansys Fluent Theory Guide 19.0*. Canonsburg, PA: ANSYS; 2018.
- Zilic de Arcos F, Vogel C, Willden RHJ. Hydrodynamic modelling of flexible tidal turbine blades. In: Proceedings of the Thirteenth European Wave and Tidal Energy Conference Vicinanza D, ed. Università degli Studi della Campania "Luigi Vanvitelli" EWTEC; 2019; Italy:2309-1983. ISSN.
- Johansen J, Sørensen NN. Aerofoil characteristics from 3D CFD rotor computations. *Wind Energy*. 2004;7(4):283-294.
- Katz J, Plotkin A. *Low-Speed Aerodynamics*, Vol.13: Cambridge, UK: Cambridge University Press; 2001.

How to cite this article: Zilic de Arcos F, Vogel CR, Willden RHJ. Extracting angles of attack from blade-resolved rotor CFD simulations. *Wind Energy*. 2020;23:1868-1885. <https://doi.org/10.1002/we.2523>

APPENDIX A: STREAMTUBES AS COLLECTIONS OF STREAMLINES

Sets of 500 streamlines at different radii are used to capture the distribution of streamlines that arises in a viscous wake. The seeding plane is located at $0.5R$ downstream of the turbine plane, and 50 radial locations are considered. The streamlines are constructed in both upstream and downstream directions by integrating through the flow field using a Runge–Kutta 4-5 adaptive integration scheme. This approach allows the streamtube to be tracked even if wake mixing or flow separation occurs and to determine the variability of the radial coordinate of the streamlines at different axial locations, enabling assessment of the radial spread. Each streamline is observed to spiral into or away from the flow centreline due to radial velocity components. Hence, an initial circular streamtube distorts from the circular geometry as it evolves up or downstream (see the three-dimensional flow image in Figure A1). Figure A1 also shows the azimuthally averaged streamtubes and error bars computed as twice the standard deviation of the radial position of the streamlines. The error bars remain small showing a small spread in radii, from which we conclude that the streamtube can be approximated by its azimuthally averaged position.

FIGURE A1 Streamtubes built from the collections of streamlines for the Sch15B rotor at $\lambda = 5.5$. Streamtubes shown in right image are azimuthally averaged, and error bars are two standard deviations of the radial position of the streamtube [Colour figure can be viewed at wileyonlinelibrary.com]



Following this analysis, a comparison of the angle of attack calculated with the azimuthally averaged streamtubes (integrated with fourth-order Runge–Kutta) and the streamlines tracking approach for all the tip speed ratios and at interpolating the velocities at two chordwise distances ($x/c = 1.0$ and $x/c = 2.0$) is shown in Figure A2. The two methods show an excellent agreement except for the tip region, proving the streamtubes approach as a viable estimation to include the expansion of the streamtubes in the azimuthally averaged field determination.

FIGURE A2 Comparison between the angles of attack extracted with the sets of streamlines and the azimuthally averaged streamtubes. The velocities were extracted at $x/c = 1.0$ (left) and $x/c = 2.0$ (right) from the turbine plane on both cases [Colour figure can be viewed at wileyonlinelibrary.com]

